frontiers | Frontiers in Energy Research

ORIGINAL RESEARCH
published: 20 April 2022
doi: 10.3389/fenrg.2022.888303

Impact of Mono- and Dual-Sized α-Fe_2O_3 Catalyst Mixtures on the Thermochemical Processing of Pinewood for Upgraded Liquid Chemicals

Adel Baimoldina[1], *Konstantinos Papadikis*[2]* *and Elena Yu. Konysheva*[3]

[1]Department of Chemistry, Xi'an Jiaotong-Liverpool University, Suzhou, China, [2]Department of Civil Engineering, Xi'an Jiaotong-Liverpool University, Suzhou, China, [3]Institute of Metallurgy of the Ural Branch of the Russian Academy of Sciences, Ekaterinburg, Russia

The incorporation of mono-sized particle catalysts in real industrial systems for biomass conversion is a significant challenge, hence the impact of individual α-Fe_2O_3 catalysts with varying non-ideal spherical sizes of 54 nm (FS054), 221 nm (FS221), and ~2 μm (FSm002) as well as dual-sized mixtures (FS054-FS221 and FS221-FSm002) were considered in the catalytic upgrading of pinewood pyrolysis vapors. The size variation of the α-Fe_2O_3 catalyst revealed a substantial effect on the product distribution. Although the yield of phenols shows a decrease by almost a factor of two irrespective of the catalyst particle size, the FS221 catalyst demonstrates the most potent effect on reducing phenols through decarboxylation reactions. Considering the role of the catalyst on the individual phenolics, the FS221 catalyst reveals higher selectivity towards the reduction of 2-methoxyphenol, isoeugenol, and eugenol, whereas the application of FS054 catalysts displays a stronger impact on the decrease of creosol and other phenols. Both FS054 and FS221 catalysts showed the highest effectiveness in reducing the relative yield of 2-methoxy-4-vinylphenol. Applying a dual-size mixture (FS054-FS221) shows a synergetic effect, simultaneously decreasing the content of phenols, acids, and aldehydes followed by a strong CO_2 release attributed to competitive decarbonylation reactions of aldehydes. The appearance of γ-Fe_2O_3 small fraction was revealed in the powders with mono-(FS221) and dual particle size (FS054-FS221 and FS221-FSm002), whereas the FS054 and FSm002 catalysts demonstrate good chemical and phase stability.

Keywords: α-Fe_2O_3 (hematite), mono and dual particle size catalyst, non-ideal spheres, thermochemical processing, upgraded liquid chemicals

OPEN ACCESS

Edited by:
Mohammad Rehan, King Abdulaziz University, Saudi Arabia

Reviewed by:
Wasif Farooq, King Fahd University of Petroleum and Minerals, Saudi Arabia
Halil Durak, Yüzüncü Yıl University, Turkey

***Correspondence:**
Konstantinos Papadikis
Konstantinos.Papadikis@xjtlu.edu.cn

Specialty section:
This article was submitted to Bioenergy and Biofuels, a section of the journal Frontiers in Energy Research

Received: *02 March 2022*
Accepted: *31 March 2022*
Published: *20 April 2022*

Citation:
Baimoldina A, Papadikis K and Konysheva EY (2022) Impact of Mono- and Dual-Sized α-Fe_2O_3 Catalyst Mixtures on the Thermochemical Processing of Pinewood for Upgraded Liquid Chemicals. Front. Energy Res. 10:888303. doi: 10.3389/fenrg.2022.888303

INTRODUCTION

The utilization of renewable energy sources has become an absolute necessity as the limited fossil resources cannot sustainably meet the fast-growing energy sector's increasing demands. Most importantly, however, the adverse environmental effects of the latter and the already visible impact on climate change have accelerated global efforts to exploit various forms of alternative energy (geothermal, wind, ocean, nuclear, solar, fuel cells and biomass). Biomass residues constitute a

clean energy source with potentially negligible NO_x, SO_2, and soot emissions due to negligible contents of sulfur, nitrogen, and ash. Moreover, biomass is considered a carbon-neutral energy source, as CO_2 emission is recirculated in the atmosphere through the plant photosynthetic reactions. The enormous global biomass resources (146 milliard metric tons a year), as well as its sustainable carbon-containing nature, make this specific source of energy a desirable alternative for the production of gaseous and liquid fuels and value added-chemicals (Lynd, et al., 1991; Zhang et al., 2007).

Fast pyrolysis has been one of the most significant thermochemical routes for converting woody biomass into liquid fuels or value-added chemicals. It refers to the rapid thermal decomposition of lignocellulosic biomass in an inert atmosphere at moderate temperature (400–500°C) with a short vapor residence time, resulting in the production of bio-oil, gases and char (Isahak et al., 2012). Bio-oils produced through the fast pyrolysis process constitute a complex mixture of oxygenated hydrocarbons with undesirable properties, such as high viscosity, chemical instability, corrosiveness, high ash content, and others (Li et al., 2021). This makes the direct use of such bio-oils in industrial applications extremely challenging. *In-situ* catalytic upgrading of fast pyrolysis vapors with subsequent liquefaction has been identified as a feasible method for reducing the yields of undesired compounds in the final liquid product. This is achieved through a series of chemical reactions and mechanisms promoted by the applied catalyst on the pyrolysis products. In order to obtain a final product with reduced oxygen content, liquid bio-oil hydrotreatment is typically followed.

Pyrolysis studies have provided a significant insight on the thermal decomposition routes and mechanistic behaviour of different types of biomass, as well as on the effect of catalyst, temperature and thermal pre-treatment on the final product distribution (Demirbas, 2000; Bridgwater, 2012; Aysu and Durak, 2015; Yücedağ and Durak, 2019; Alayont et al., 2022). Thermal decomposition of holocellulose (cellulose and hemicellulose) primarily results to volatile components due to the decomposition of sugars, while the decomposition of lignin primarily results to char and phenolics. Gradually increasing the pyrolysis temperature, a progression from carbonization (charcoal formation at low temperatures, ~400°C), to devolatilization that favours liquid formation (moderate temperatures and short residence time, ~500°C) and finally to increased non-condensable gas formation (high temperatures and long residence times, ~750–900°C) is observed (Bridgwater, 2012). During carbonization, depolymerization reactions, CO, CO_2, and free radicals through various decomposition mechanisms result in an increased solids content. The formation of pyrolysis vapors, which is typically followed by rapid quenching for liquid products, proceeds through a series of reactions; 1) cellulose fragmentation at high temperatures (carbonyl compounds), depolymerisation at moderate temperatures (anhydrosugars) and dehydration at lower temperatures (gases, water, char), 2) hemicellulose decomposition in a similar way to cellulose, 3) lignin decomposition through dehydration at lower and moderate temperatures and lignine monomer formation at moderate and higher temperatures (Velden et al., 2010; Alayont et al., 2022). At high temperatures, tar cracking reactions dominate the process leading to increased formation of non-condensable gaseous products. Generally, cracking of reactive intermediates with increased hydrogen and CO yields is promoted at higher temperatures, while a decrease in CO_2 is also observed (Hu and Gholizadeh, 2019).

Iron oxides are increasingly considered as a potentially feasible catalyst for the *in-situ* catalytic fast pyrolysis of biomass for several attractive operating (e.g., environmentally friendly and highly efficient) and economic (e.g., readily available and inexpensive) features (Schwertmann and Cornell, 2000; Zheng et al., 2006). α-Fe_2O_3 (hematite), among other Fe_2O_3 polymorphs, displays the best thermal and chemical stability under ambient conditions (Machala et al., 2011; Tuček et al., 2015) and has been extensively used in various areas of catalytic applications such as reduction/oxidation and acid/base reactions (Jia et al., 2015), oxidation of CO (Walker et al., 1988), coal volatiles upgrading (Song et al., 2022), photocatalytic water oxidation (Meng et al., 2013), the biodegradation reactions of green algae (Fouad et al., 2019), for catalytic degradation of organic pollutants (Rufus et al., 2019), and others.

Although a high catalytic activity is primarily linked to large surface area and diversity of surface defects of the catalyst particles, additional parameters have also been found to contribute to the increased catalytic activity of α-Fe_2O_3. Factors, such as phase evolution and grain morphology, pore size distribution, bandgap width, etc., are just a few of those. α-Fe_2O_3 (hematite) has been a catalyst that has received increased attention primarily due to its multivalent nature, reduction/oxidation, and acid/base properties, as well as due to its wide availability, thermal and chemical stability, and inherently low cost (Liu et al., 2014). Zhang et al. (2014) proposed a catalyst for bio-oil upgrading based on Fe_2O_3 supported onto CaO that promoted the yields of furans and light aromatic hydrocarbons at the expense of acids and aldehydes/ketones. Lim et al. (2014) applied the industrial by-product of the aluminium industry, Red Mud (a mixture of 30–60% Fe_2O_3 with TiO_2, Al_2O_3, CaO, and SiO_2), in the CFP of different types of biomass. It was found that the application of Fe_2O_3 in biomass CFP resulted in the decrease of heavy compounds in the bio-oil due to red/ox reactions at 500°C (Torri et al., 2010). More recently, Weber et al. (2019) tested different catalysts originating from Red Mud treatment and reduction at varying temperatures with catalyst particle size in the range of 0.5–2 mm. The investigation revealed a strong potential for using iron oxide (magnetite) based catalysts doped with alkali metals to promote the ketonization of fast pyrolysis oxygenates with limited coking. After acid treatment of Red Mud, the ketonization activity of the obtained catalysts was limited, giving rise to more intense coking due to the lack of alkali metals and subsequently base sites. Similarly, Kastner et al. (2015) investigated the effect of activated Red Mud, a catalyst composed primarily of magnetite with particle size in the range of 1.5–2 mm, on the upgrading reactions of biomass pyrolysis model compounds. It was found that activated Red

Mud also promoted the ketonization reactions of model compounds in a manner similar to a mixed metal oxide catalyst.

The application of iron oxides in CFP has primarily promoted decarboxylation reactions, decreasing the overall condensed liquid bio-oil yield. However, the quality of the final obtained liquid product is significantly improved with increased potential in meeting the requirements for practical applications. Although micron-sized α-Fe_2O_3 has been investigated as a potential catalyst for CFP, there is a lack of systematic studies focusing on applying nano-sized catalysts and in particular mixtures of single-sized catalysts (giving dual-sized catalyst of the same chemical origin). Only a limited number of results for nano-sized iron oxides have been presented in the pyrolysis of poplar wood biomass (Lu et al., 2010). However, there is no detailed investigation on the final product distribution after CFP, whilst it is also not evident from the presented discussions whether α-Fe_2O_3 or γ-Fe_2O_3 polymorphs were the applied catalyst. Baimoldina et al. (2019) also investigated the effect of α-Fe_2O_3 nano-sized and micro-sized catalysts with different shapes on the product distribution in the CFP of pinewood. It was identified that catalyst shape profoundly affected the distribution of phenols, aldehydes, ketones, acids, and CO_2. Interestingly, spherical-like nano-sized and octadecahedral (≈0.5 microns) catalyst particles promoted the formation of acetaldehyde, whereas the octadecahedron shape resulted in the complete elimination of heavy acids. In addition, the reduction of phenols correlated well with the increase in CO_2 production during the process.

The present study explores the effect of α-Fe_2O_3 with different particle sizes for non-ideal spheres (from 54 nm to 2 μm) on the catalytic product distribution, derived from the fast pyrolysis of Pinewood biomass at 500°C. The impact of the α-Fe_2O_3 catalysts with different sizes is analyzed using the Py-GC/MS (pyrolysis-gas chromatography-mass spectrometry) technique.

MATERIALS AND METHODS

Materials

Pinewood with a particle size of 500 μm was chosen as the biomass feedstock because it was considered the optimal studying material with low ash content (Mendes et al., 2016). The small pinewood particle size was selected to ensure a thermally thin regime with negligible intra-particle temperature gradient during the pyrolysis process (Papadikis et al., 2009). Pinewood was dried at 105°C for 24 h in an oven before experiments and kept in a desiccator in a closed container. Nano α-Fe_2O_3 powder (MACKUN, China) and submicron α-Fe_2O_3 (FS221) (Aladdin, China) powder were calcined for 3 h at 800°C (FS054) and 3 h at 1000°C (FSm002), respectively, to obtain non-ideal spherical α-Fe_2O_3 with different particle sizes. α-Fe_2O_3 powders with dual particle size made of FS054 and FS221 (FS054-FS221) as well as FS221 and FSm002 (FS221-FSm002) were prepared by proper mixing in a mortar in 50:50 wt% ratio at room temperature. The powders FS054-FS221 and FS221-FSm002 were applied in CFP as obtained without preliminary thermal treatment.

Characterization

The XRD patterns were recorded on a Bruker D8 Advance diffractometer (Bruker AXS, Germany) operating with $Cu_{K\alpha}$ radiation in the range of $10 \leq 2\theta$ degrees ≤ 100 at room temperature under an air atmosphere. An FEI Tecnai G20 transmission electron microscope (TEM, FEI, United States) with the acceleration voltage of 200 kV and JEOL JSM-6510 scanning electron microscope (SEM, JEOL, Japan) in 5–30 keV energy range were used to characterize the morphology of catalysts. The BET measurements were carried out on a 3H-2000PS2 apparatus (BeiShiDe Instrument—S&T, China) in the static volumetric mode to estimate the specific surface area and pore sizes of the catalysts. 2–7 measurements were carried out for each sample. To evaluate quantitatively mesoporosity, the method developed by Barrett, Joyner, and Halenda (BJH method) (Barrett et al., 1951) was applied. The models of Horvath and Kawazoe (HK method) (Horvath and Kawazoe, 1983) as well as Dubinin and Radushkevich (DR method) (Dubinin, 1966) were used to estimate the microporosity.

In-situ fast pyrolysis analysis was performed with the Pyrolyser (CDS pyroprobe 5000 series, United States) in combination with Gas Chromatography-Mass Spectrometry (GC/MS) technique (7890A/5975C, Agilent technology, United States). For the non-catalytic pyrolysis experiments, 1 mg of biomass was positioned in a quartz tube sandwiched by layers of quartz wool. *In-situ* catalytic fast pyrolysis for vapor upgrading was studied using 1 mg of biomass and 4 mg of a catalyst properly mixed in a mortar before the final mixture was positioned into the quartz tube. As in the conventional fast pyrolysis experiments, the biomass-catalyst mixture was sandwiched between quartz wool layers. For the sake of convenience, the abbreviation "PW: catalyst" will be used for the experiments after CFP. The pyroprobe with a sample was heated at the rate of 20°C ms^{-1}–500°C. The pyrolysis process was carried out at this temperature within 20 s with a biomass-to-catalyst ratio of 1:4. Helium was used as the carrier gas with a 30 ml/min flow rate, introducing the pyrolysis vapors GC/MS system. The split ratio setting the GC/MS was 50:1, whilst the temperature of the injecting system was maintained at 300°C. The GC/MS interface temperature was held at 250°C, at a pressure of 10 psi. The chromatographic separation was performed by using 5%-phenyl-methylpolysiloxane (HP-5MS) non-polar capillary column (30 m length with 0.25 mm internal diameter). The oven temperature ramp in the gas-chromatograph was progressively increased from 50°C to 300°C at a rate of 5°C min^{-1}. The temperature of 300°C was maintained for 7 min to ensure that the column was clean from any heavy molecules. Mass spectra were obtained for m/z ratio in the range of 35–550 amu, while the GC/MS was operated at the

electron ionization (EI) mode at 1459V. Reproducibility experiments were conducted three times for each sample (non-catalytic pyrolysis and catalytic pyrolysis).

Data treatment: Chromatographic peaks were identified by comparing their mass spectra to the standard spectra of organic compounds in the NIST MS library and literature data. Each product's relative peak area percentage (%) evaluated the catalyst's impact on the pyrolysis product distribution. However, using GC/MS as the volatile compound identification method imposes certain limitations as the relative concentrations derived from the peak area percentages are a function of the individual compound's ionization ability. This paper assumes that the chromatographic peak area percentage of an individual compound is proportional to its concentration (first order approximation). Hence, the change in each compound's chromatographic peak area percentage from different experiments was used to determine the catalyst impact on the relevant yield. Moreover, the detected chemical compounds were grouped according to their main functionality by using IUPAC classification. Since each experiments was carried out three times for each sample, the average peak area and its standard deviation were evaluated for each group to indicate the spread of the obtained values. The total area is in the range of 99.9–100.1% due to automatic rounding of numbers by Excel, which was the used software for data analysis.

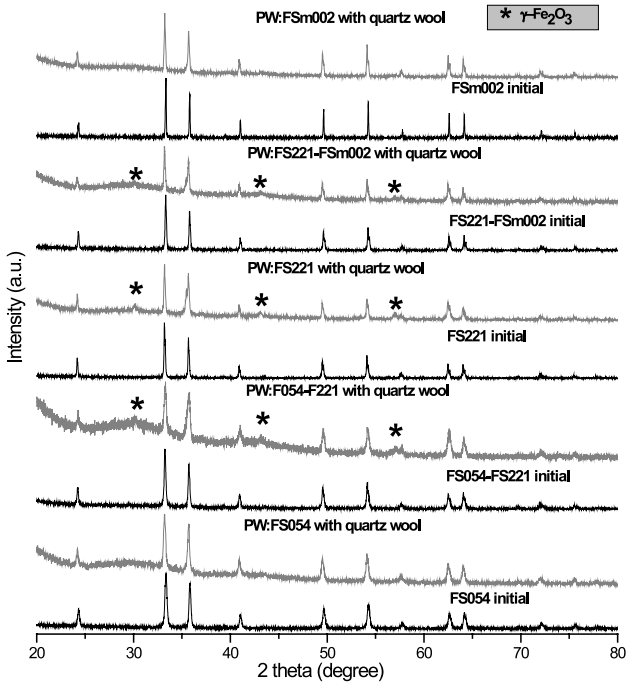

FIGURE 1 | XRD patterns of α-Fe_2O_3 with different sizes initially and after CFP. After CFP the XRD patterns of the catalysts were recorded with a small amount of quartz wool, which was used to fix a catalyst with biomass in the pyroprobe, and it was challenging to separate it without loss of catalyst.

RESULTS AND DISCUSSIONS

Chemical, Structural, and Morphological Stability of the α-Fe_2O_3 Catalysts With Different Sizes Initially and After CFP

Initially, all spherical-like α-Fe_2O_3 powders independent of the particle size were single-phase with a hematite crystal structure (**Figure 1**). The particle size for the powders was calculated from the TEM and SEM images (**Figure 2** and **Table 1**). The specific surface area of powders decreases by about 8 times with the rise in the size of powders (from nano to micron size). Micro-, meso-, and macroporosities coexist in the powders. The BET measurements can quantitatively describe microporosity and mesoporosity (**Table 1**). The mesoporosity estimated by the BJH method is noticeably larger than the microporosity defined by the HK and DR methods. The absolute values of both mesoporosity and microporosity decrease, respectively, by about 4 times and 15–19 times with the rise in the particle size from 54 nm to 2 μm, but their ratio becomes larger for the micron-sized FSm002 catalyst (**Table 1**). According to the literature (Liang et al., 2022), the acidity of α-Fe_2O_3 catalysts decreases with the particle size and crystallinity increase.

In addition, the α-Fe_2O_3 catalysts with different sizes were initially characterized by XPS to describe the surface chemical states of O, Fe, C, and their surface concentrations (**Tables 2**, **3** and **Figures 3**–**5**). Carbon was found at the surface of all materials. The total concentration of carbon at the surface of FS054 is almost two times higher comped to FS054-FS221, FS221, and FS221-FSm002 catalysts. The three contributions can be distinguished in the C1s XPS spectra with the strongest contribution at E_{BE} = 284.6 eV that can be related to C-C and C-H bonds (**Figure 3A**, **Figure 4A**). This contribution is the strongest in the C1s XPS spectrum of FS054. The less intense contribution at E_{BE} = 286.1 eV is slightly larger for the single-sized FS054, whereas the contributions at E_{BE} = 288.4–288.8 eV are comparable to all catalysts. The surface concentrations of iron and oxygen in FS054 are lower than for other catalysts by 7.2–10.4 at% and 4.8–9.2 at%, respectively. The highest Fe surface concentration was revealed in the dual-sized FS221-FSm002 catalyst (29.1 at%), but it is still lower by 10.9 at% compared to the expected one according to the nominal stoichiometry. The highest oxygen surface concentration was detected for the dual-sized FS054-FS221 catalyst, and it is comparable with the nominal stoichiometry. Comparing the surface concentrations estimated by XPS with the nominal stoichiometry of α-Fe_2O_3, one could suggest that the carbon at the surface of catalysts is preferably located on the iron sites and demonstrates the following trend: the carbon concentration decreases with increasing the particle size (**Table 2**). However, if one looks at the re-distribution of carbon over the surface between assumed ideal oxygen and iron surface sites, FS054-FS221 catalyst demonstrates a significantly different result: carbon location over the O and Fe sites is 1:7.4, whereas it is around 1:2 for other catalysts. The [O]/[Fe] atomic ratio at the surface is always

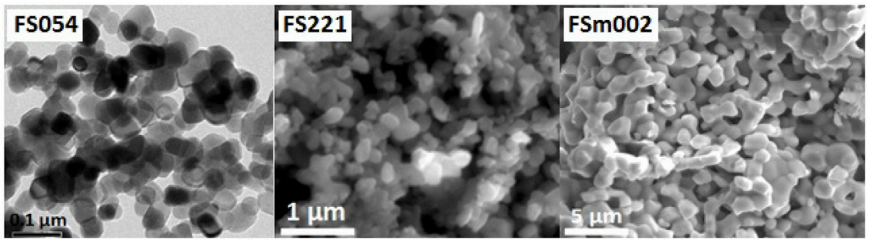

FIGURE 2 | TEM and SEM images of initial α-Fe_2O_3 with different particle sizes.

TABLE 1 | Surface area, particle size, pore volume of α-Fe_2O_3 spherical-like powders with different sizes.

Abbreviation	S_{BET} (m^2g^{-1})	[a]Particle size (nm)	BJH pore volume on desorption (ml g^{-1})	HK micropore volume (ml g^{-1})±0.0001	DR micropore volume (ml g^{-1})±0.0001	BJH/DR pore volumes' ratio
FS054	15.8 ± 0.2	54.1 ± 14.2	0.1579 ± 0.0026	0.0058	0.0060	26.3
FS054-FS221	10.6 ± 0.3	[b]54.1–220.8 [c](1: 4.1)	0.1115 ± 0.0021	0.0038	0.0040	27.9
FS221	5.6 ± 0.3	220.8 ± 57.5	0.0805 ± 0.0034	0.0017	0.0017	47.4
FS221-FSm002	4.1 ± 0.4	[b]220.8–2083.3 [c](1: 9.4)	0.0782 ± 0.0024	0.0010	0.0010	78.2
FSm002	1.9 ± 0.6	2083.3 ± 724.8	0.0405 ± 0.0156	0.0003	0.0004	101.3

[a]*Calculated for 100 particles from the TEM/SEM images.*
[b]*It was not determined for α-Fe_2O_3 powders with a dual particle size as they were fabricated at room temperature from powders with two different particle sizes and were applied in CFP as obtained (without preliminary thermal treatment);*
[c]*The ratio of the diameters of the particles.*

TABLE 2 | Elemental surface composition of catalysts from the XPS analysis.

Catalyst	Surface concentration, at%			Assumed location of carbon on surface sites, at%			Atomic ratio		
	C	O	Fe	O	Fe	O:Fe ratio	[C]/[Fe]	[C]/[O]	[O]/[Fe]
Fe_2O_3	—	60	40	—	—	—	—	—	1.5
FS054	32.4	48.9	18.7	11.1	21.3	1 : 1.9	1.7	0.7	2.6
FS054-FS221	16.0	58.1	25.9	1.9	14.1	1 : 7.4	0.6	0.3	2.2
FS221	16.9	54.2	28.9	5.8	11.1	1 : 1.9	0.6	0.3	1.9
FS221-FSm002	17.2	53.7	29.1	6.3	10.9	1 : 1.7	0.6	0.3	1.8

TABLE 3 | The concentration of Fe in different chemical states (in at%) from $Fe2p_{3/2}$ XPS spectra.

Catalyst	Defects 708.0–708.3 eV	Multiplets 709–713 eV				Surface states 713.4–714.0 eV	Satellite 718.1–718.3 eV
FS054	0.17	1.8	2.4	1.8	1.2	2.2	2.3
FS054-FS221	0.25	2.3	3.2	2.5	1.7	2.9	3.6
FS221	0.28	2.5	3.6	2.7	1.8	3.4	4.0
FS221-FSm002	0.25	2.3	3.5	2.7	1.9	3.3	4.1

higher than the expected one for the nominal stoichiometry, and it increases gradually with the decrease in the particle size, reaching the maximum value of 2.6 for FS054. The three components can be identified in the O1s XPS spectra of initial catalysts (**Figure 3B**). The component assigned to the bulk oxygen at E_{BE} = 529.3–529.7 eV is the strongest

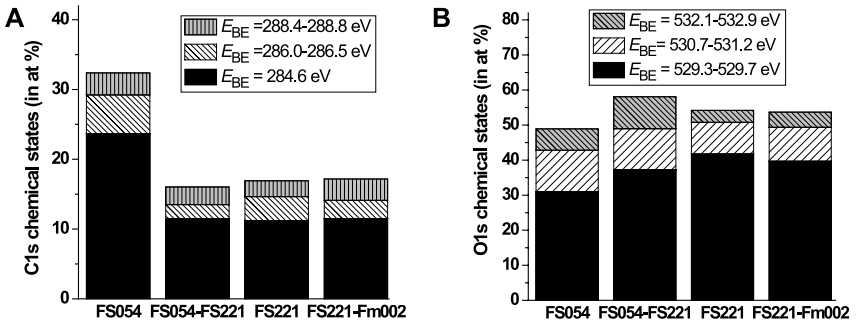

FIGURE 3 | Coexistence of different chemical states at the surface of initial catalysts according to XPS: **(A)** C1s; and **(B)** O1s.

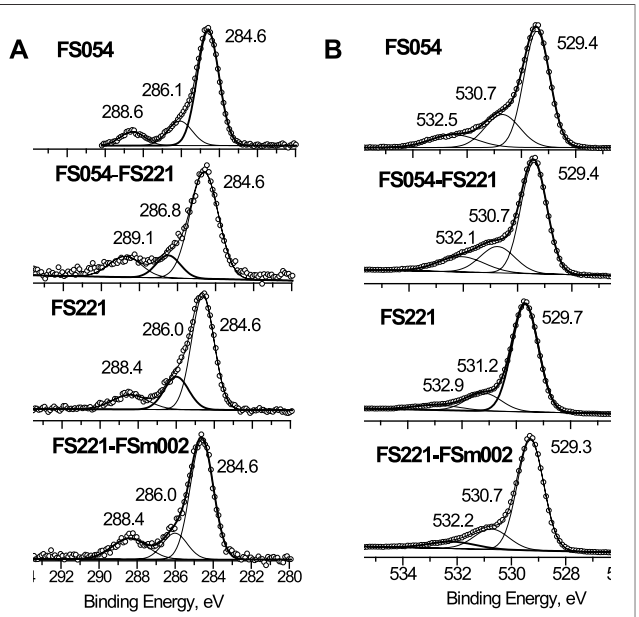

FIGURE 4 | C1s **(A)** and O1s **(B)** XPS spectra of catalysts before CFP.

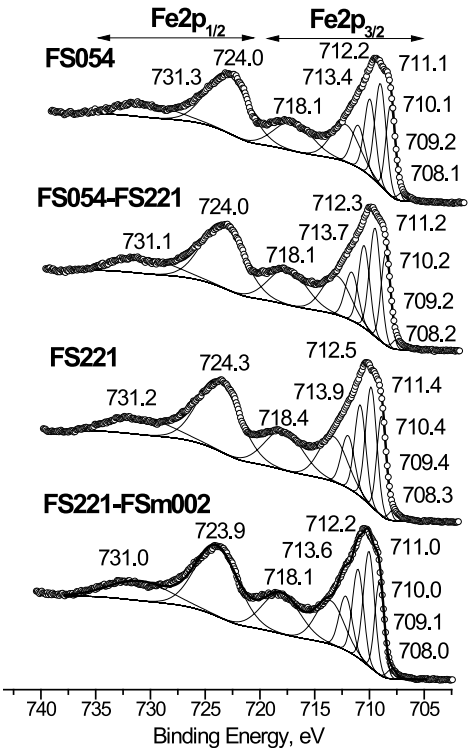

FIGURE 5 | Fe2p XPS spectra of catalysts before CFP.

for FS221 and the smallest for FS054. The contribution at E_{BE} = 530.7–531.2 eV can be associated with oxygen in the OH surface hydroxyl (Yamamoto et al., 2010), and it is larger by around 2 at% for FS054 and FS054-FS221 compared to FS221 and FS221-FSm002 catalysts (**Figure 3B**, **Figure 4B**). The contribution at E_{BE} = 532.1–532.9 eV related to adsorbed water molecules (Yamamoto et al., 2010) is stronger for FS054-FS221 and FS054 catalysts.

One can distinguish several contributions in the Fe2p XPS spectra of α-Fe_2O_3 with different sizes (Grosvenor et al., 2004), summarised in **Table 3**. The Fe2p XPS spectra of α-Fe_2O_3 with different particle sizes generally look similar for all four samples. However, all peaks in the Fe2p XPS spectrum of FS221 are slightly shifted to higher binding energy than those for FS054, FS054-FS221, and FS221-FSm002 (**Figure 5**), suggesting a longer retention time for physisorbed molecules during PW pyrolysis. The values for defects and for four components associated with Fe^{3+} 2p3/2 multiplets at 709–713 eV are comparable for the three FS221-based catalysts. The surface states and satellites increase gradually with the rise in the size of catalysts. The concentration of defects (at 708.0–708.3 eV) appearing near the sites with Fe ions in lower oxidation states (Heinrich and Cox, 1994), is lower by almost one order of magnitude, compared to other components, for all catalysts independently of their size and whether they are single-sized or dual-sized.

The absence of a strong peak at 25° 2θ in the XRD patterns of all catalysts after CFP, suggests the negligible formation of the crystalline carbon (Machado et al., 2013; Xu et al., 2017) or below 3 mol% considering the XRD detection limit. The peaks related to

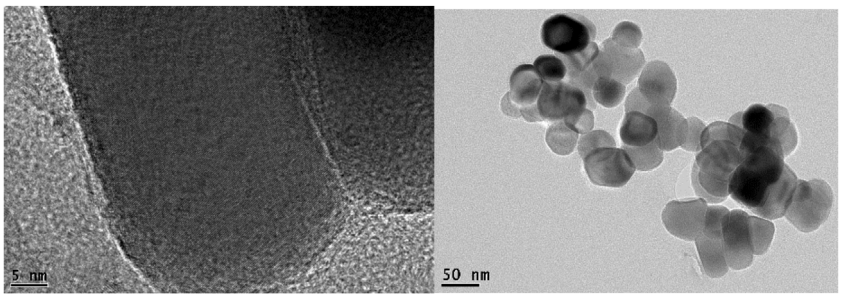

FIGURE 6 | TEM images of PW:FS054 at different magnifications.

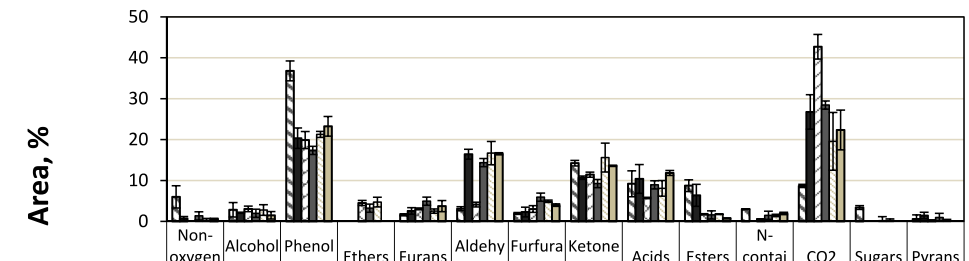

	Non-oxygenated	Alcohols	Phenols	Ethers	Furans	Aldehydes	Furfural	Ketones	Acids	Esters	N-containing	CO2	Sugars	Pyrans
PW	6.0	2.8	36.8	0.0	1.6	3.1	1.9	14.2	9.2	8.7	3.0	8.7	3.4	0.6
PW:FS054	0.7	2.1	20.3	0.0	2.6	16.4	2.3	10.7	10.4	6.4	0.0	26.8	0.0	1.4
PW:FS054-FS221	0.0	3.0	19.9	4.5	3.1	4.1	3.0	11.4	5.7	1.8	0.5	42.7	0.0	0.3
PW:FS221	1.4	2.0	17.3	3.2	4.9	14.4	5.9	9.3	8.9	1.6	1.5	28.5	0.2	1.0
PW:FS221-FSm002	0.3	2.8	21.3	4.7	2.5	16.7	4.9	15.6	8.1	1.7	1.5	19.6	0.3	0.2
PW:FSm002	0.6	1.5	23.2	0.0	3.7	16.5	4.0	13.6	11.8	0.7	1.9	22.4	0.0	0.0

FIGURE 7 | Effect of α-Fe_2O_3 size on the PW CFP products distribution.

iron carbide were not detected. After CFP, only the initial α-Fe_2O_3 phase was revealed in the PW:FS054 and PW:FSm002, suggesting good chemical and phase stability of FS054 and FSm002 catalysts. The TEM image of PW:FS054 illustrates that, after the CFP, the nano-sized PW:FS054 catalyst retains its original size (**Figure 6**). This is very promising, in particular, for nano-sized FS054 as typically nanomaterials tend to sinter or agglomerate at intermediate or high temperatures. In contrast, FS221-containing catalysts (PW:FS054-FS221, PW:FS221, PW:FS221-FSm002) were partly converted into γ-Fe_2O_3 polymorph with both Fe^{2+} and Fe^{3+} cations compared to only Fe^{3+} cations in α-Fe_2O_3. Another important difference between these polymorphs is that the stoichiometry of γ-Fe_2O_3 can be presented as $Fe(Fe_{5/31/3})O_4$, suggesting the existence of cation vacancies. The appearance of γ-Fe_2O_3 is unexpected as α-Fe_2O_3 phase is the most stable polymorph. It is known that several factors can induce the Fe_2O_3 polymorph transformations in general: particle size, single-phase or composite system, shape of crystals, temperature, and pressure et al. (Machala et al., 2011). However, typically these transformations occur from a less stable polymorph to a more stable one. If the particle size would be the key point it is not clear why only α-Fe_2O_3 was revealed in PW:FS054 with a smaller particle size than FS221-based catalysts. One may suggest that the partial irreversible transformation of α-Fe_2O_3 to a less stable γ-Fe_2O_3 polymorph is associated with the catalytic activity of the iron cations in the reduction process and occurring of the oxidation processes during the catalytic vapor upgrading, in particular, phenols. Note that iron nanotubes were also partially converted to the less stable γ-Fe_2O_3 during the CFP and demonstrate the best performance in the phenolics reduction among other catalysts explored (Baimoldina et al., 2019). A partial reduction of iron cations followed by transformation from α-Fe_2O_3 to γ-Fe_2O_3 may be promoted due to CO and H_2 formation during the pyrolysis as well, but there is no information about the difference in CO and H_2 concentrations over different catalysts. This partial structural transformation may also be associated with ether formation in a small quantity (3.2–4.7%, **Figure 7**) as it was observed for the same catalysts, for which γ-Fe_2O_3 in a small quantity was detected after CFP. According to XPS, there is an enrichment in oxygen or, alternatively, a deficiency in iron cations at the surface within a few nanometers for all catalysts (**Table 2**). Based on these observations, the surface and the near surface region should be involved for such structural transformation to be triggered. On

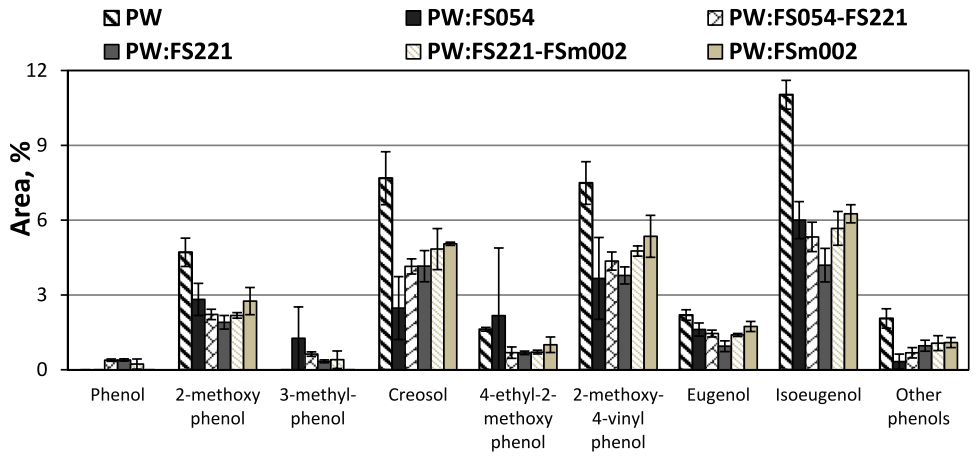

FIGURE 8 | Effect of mono- and dual-sized α-Fe_2O_3 catalyst particle mixtures on the PW CFP phenols distribution.

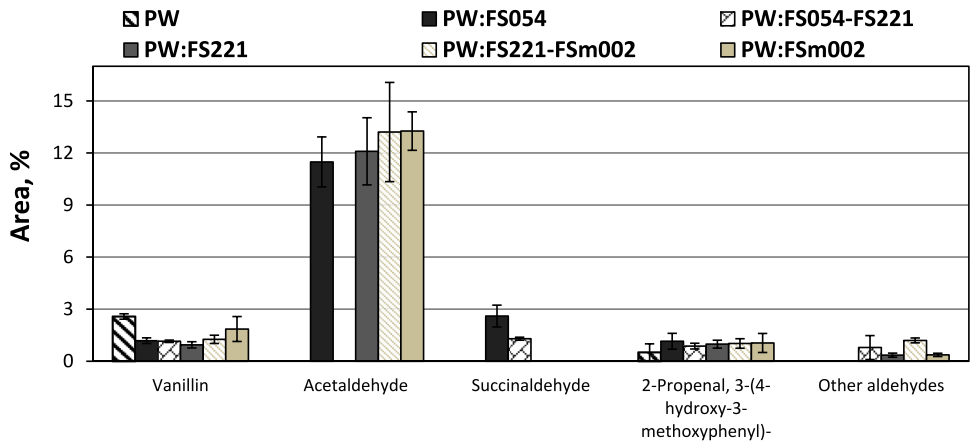

FIGURE 9 | Effect of mono- and dual-sized α-Fe_2O_3 catalyst particle mixtures on the PW CFP aldehyde distribution.

the other hand, these additional layers with an excess of oxygen could be built over an iron oxide catalyst through the physisorption of small, oxygen-containing fragments of biomass decomposition. When a specific critical value is reached, the phase transition from α-Fe_2O_3 to γ-Fe_2O_3 could occur.

Fast Pyrolysis of Pinewood

Woody biomass comprises a mixture of biopolymers, such as cellulose, hemicellulose, and lignin at varying proportions, depending on the biomass origin and nature. The rate of decomposition and temperature range for these biopolymers vary, and, depending on the reaction atmosphere, the resulting products span a wide range of chemical groups at different proportions. Cellulose and hemicellulose are typically associated with the production of alcohols, ethers/esters, furans/furfural, aldehydes/ketones, and acids, whilst lignin is the primary source for phenolic compounds. The GC/MS chromatogram for the conventional pyrolysis of pinewood contains more than 110 peaks. The identified fast pyrolysis compounds were grouped into non-oxygenated compounds, alcohols, phenols, ethers, furans, aldehydes, furfural, ketones, acids, esters, nitrogen-containing compounds (N-containing). Non-oxygenated compounds refer to the detected oxygen-free compounds.

Initial high relative peak areas were present for the groups of phenols, ketones, acids, esters, and CO_2, whilst the overall picture is significantly different after applying the catalysts for the groups of phenols, aldehydes, and CO_2. The relative area for the phenolic compounds amounted to a total of 36.8%, originating from the decomposition of lignin. The relative peak areas of acids and ketones amounted to 9.2% and 14.2%, respectively. The formation of esters, non-oxygenated compounds, and CO_2 are associated with more complex decomposition reaction routes catalysed by the presence of inorganics existing initially in pinewood (Liu et al., 2014). In this study, it is assumed that

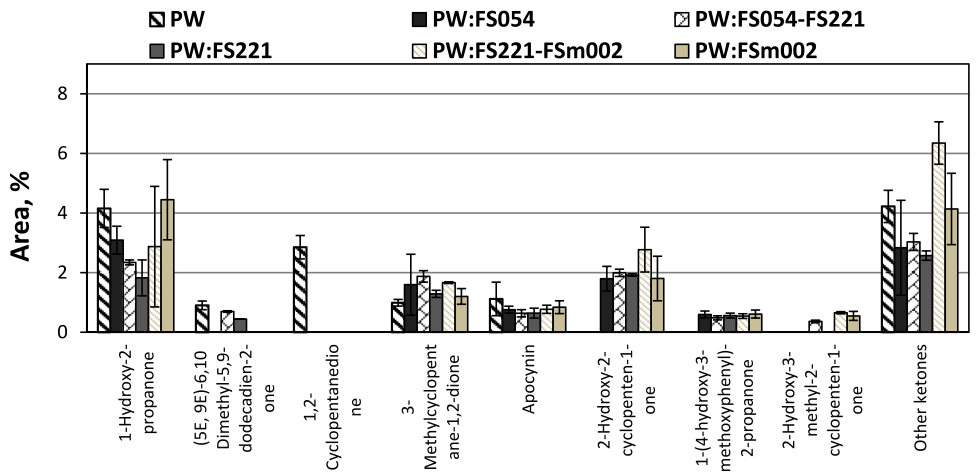

FIGURE 10 | Effect of mono- and dual-sized α-Fe_2O_3 catalyst particle mixtures on the PW CFP ketones distribution.

the changes in the relative chromatographic area are proportional to the changes in concentration. However, changes in the relative peak area of the fast pyrolysis products also depend on the individual compounds' ionisation ability; hence, this is considered a first-order approximation in the following analysis.

Impact of Mono- and Dual-Sized α-Fe_2O_3 Catalyst Particle Mixtures on the Product Distribution on Pinewood Pyrolysis

Figure 7 shows the effect of the mono- and dual-sized α-Fe_2O_3 catalyst particle mixtures on the product distribution of the CFP of pinewood. Phenols, aldehydes, esters, and CO_2 are the primarily affected chemical compound groups with significant variations in their relative peak area for the different catalyst sizes and combinations.

A noticeable reduction in the relative peak area of the phenolic group is observed for all applied catalysts sizes that correspond to approximately half of the initial relative peak area magnitude. No specific particle size or mixture shows a significant deviation in the phenols reduction pattern observed during CFP. All applied catalysts displayed a substantial increase in the formation of aldehyde compounds apart from the nanosize dual particle mixture of FS054-FS221, which showed no effect on promoting the formation of aldehyde compounds compared to pure pinewood pyrolysis. This is an interesting outcome, especially when correlated to the significant increase in CO_2 observed for this specific catalyst particle mixture, and it is further discussed below. The relative peak area of the esters group is significantly reduced for all applied catalysts apart from the monosized FS054, which had a minor effect in the reduction of esters compared to pure pinewood, while the appearance of ether compounds is linked to all catalysts containing the FS221 particle group. Finally, a significant increase in the formation of CO_2 is observed for all catalysts at relatively comparable levels. The FS054-FS221 mixture shows a different pattern with a relative peak area of approximately five times higher than that of the original pinewood pyrolysis. The increase in CO_2 is typically an indicator of decarboxylation and decarbonylation reactions, followed by water-gas shift reactions promoted by Fe_2O_3, associated with the conversion of various chemical groups (acids, ketones, phenols, etc.) over transition metal oxides (e.g., Fe_2O_3).

As a general observation, it is found that α-Fe_2O_3 suppresses the formation of phenolic compounds and leads to increased CO_2 formation through various reaction pathways. The impact of α-Fe_2O_3 catalysts on aldehydes, esters, and ethers shows a size or mixture-dependent behavior indicative of particle-size-dependent selectivity in the catalytic degradation reactions of fast pyrolysis vapors.

Impact on the Distribution of Phenolic Compounds

The impact of the applied catalysts with different particle sizes and mixtures within the phenolic group is shown in **Figure 8**. The individual phenolic compounds that have been most substantially affected are 2-methoxyphenol (i.e., guaiacol), 2-methoxy-4-methylphenol (i.e., creosol), 2-methoxy-4-vinylphenol, and 2-methoxy-4-(prop-1-en-1-yl)phenol (i.e., isoeugenol).

In terms of relative peak areas, the FS054 showed the strongest impact in the decrease of the formation of creosol, a compound that is progressively favored as the catalyst particle size increases. The FS054-FS221 and FS221 catalysts display generally similar behavior. However, the FS221 revealed a higher selectivity towards the reduction of isoeugenol, eugenol and 2-methoxy-4-vinylphenol, whereas the application of FS054 catalyst has a more substantial impact on the decrease of creosol and other phenols. Both monosized nanoparticle catalysts, FS054 and FS221, showed the highest effectiveness in decreasing the relative yield of 2-methoxy-4-vinylphenol. The FSm002 generally had the smallest impact on reducing the individual phenolic compounds, however, its overall effect is still noticeable and more intense on heavier phenolics, such as isoeugenol.

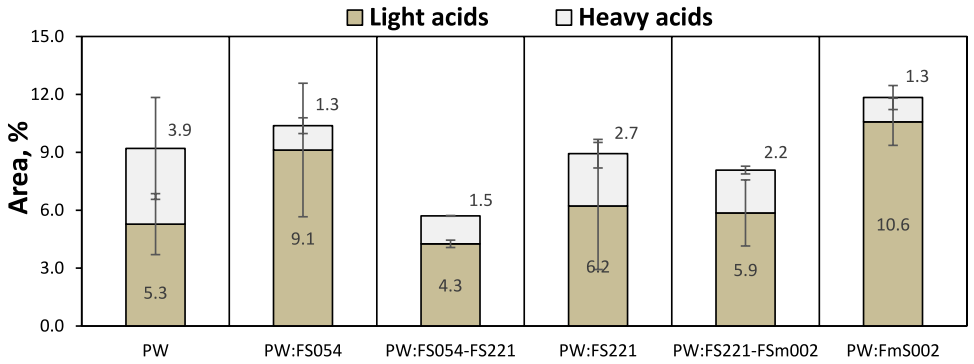

FIGURE 11 | Effect of α-Fe_2O_3 particle size on the distribution of acids after CFP of PW. Aliphatic acids with C < 4 were classified as light acids, whereas aliphatic and cyclic acids with C > 4 were grouped as heavy acids.

The overall impact of α-Fe_2O_3 on the catalytic decomposition of the phenolic compounds can be primarily focused on the suppression of their formation with associated release of CO_2 as shown in **Figure 7**. Considering that the degradation of phenolics over hematite catalysts does not lead to a significant amount of new phenolic products, it can be speculated that α-Fe_2O_3 favors the formation of radicals during lignin degradation that further enable char formation, as well as coking along the OCH_3 rearrangement pathway primarily from guaiacols (Gupta et al., 2017; Kawamoto, 2017). Although there are clear indications of the impact of catalyst particles size on the suppression of phenolic compounds, the trends tend to differ depending on molecule structure. The appearance of new phenols for nano-sized catalyst particles and mixtures, i.e., phenol for all FS221 containing catalysts and 3-methyl-phenol for FS054 and all FS221 containing catalysts, shows that nanoparticle size catalysts with increased spherical symmetry further promote demethoxylation and side-chain cracking reactions. At the same time, the formation of 3-methylphenol (i.e., m-cresol) can be attributed to the promotion of the homolytic cleavage of the O–CH_3 bond and radical-induced rearrangements (Asmadi et al., 2011; Kawamoto, 2017).

Impact on the Distribution of Aldehyde Compounds

All applied catalysts showed a significant increase in the relative peak area of aldehyde compounds, apart from the nanosize catalyst mixture FS054-FS221, which showed almost no effect on the aldehyde compound group distribution. This increase is primarily associated with the formation pathway of acetaldehyde (**Figure 9**), a compound absent from the products of pure pinewood pyrolysis. Interestingly, acetaldehyde formation was not a promoted reaction pathway for the FS054-FS221 catalyst. Additionally, the FS054-FS221 catalyst displays a significantly higher release of CO_2 (**Figure 7**) than any other catalyst.

Considering the effect of α-Fe_2O_3 on the aldehyde group, it can be hypothesized that highly symmetric nano- and micro-sized catalyst particles strongly promote the formation of acetaldehyde, possibly through the cellulose decomposition pathway and, more specifically, the catalytic decomposition of levoglucosan (Zhang et al., 2012). Two possible reasons could be identified for the diverse behavior of the FS054-FS221 mixture to catalyze the levoglucosan decomposition pathway to acetaldehyde; 1) the highly asymmetrical structure of the resulting mixture with a particle diameter ratio of approximately 1: 4.1, 2) an enhanced catalytic transfer hydrogenation (CTH) reaction over the carbon-rich Fe surface (**Table 2**) on the acetaldehyde carbonyl (Mabate et al., 2022). Hydrogen is present in the system during the biomass thermal decomposition reactions and through the water-gas shift reaction over Fe_2O_3.

For the former, this would mean that the catalyst mixture operates like a conical nanotube than a non-ideal sphere. This observation is also in line with the findings of Baimoldina et al. (2019), where highly anisotropic shape iron oxide nanotubes were incorporated in the catalytic conversion of pinewood. The high relative peak area of CO_2 for the FS054-FS221 catalyst could also indicate subsequent decarbonylation reactions of acetaldehyde to CH_4 and CO promoted due to the high effective catalyst shape anisotropy. The experimental setup in this study did not allow for the detection of light molecular weight compounds in the GC-MS, such as CH_4. However, the excessive relative peak area of CO_2 provides further evidence in this direction. The conversion of CO to CO_2 is highly favored over Fe_2O_3 catalysts through the water-gas shift reaction. Hence, a correlation between catalyst particle size ratios and final product distribution in dual-sized mixtures is evident and perhaps forms an essential parameter for controlling the final targeted chemicals.

In the latter case, the high carbon content on the Fe active site could further promote the CTH reaction on the terminal carbonyl of the acetaldehyde molecule. Acetaldehyde decarbonylation would produce CH_4 and CO as the reaction products through the CTH reaction. Subsequently, the water-gas shift reaction would proceed over the Fe_2O_3 catalyst in a similar fashion as mentioned previously.

In contrast, the FS221-FSm002 catalyst mixture with a particle diameter ratio of approximately 10:1 did not display similar behavior to FS054-FS221. It promoted the formation of acetaldehyde similar to the monosized catalysts FS054 and FS221. The anisotropic shape and the highest surface oxygen concentration of FS054-FS221 could probably play an additional role.

Impact on the Distribution of Ketonic Compounds

The general impact of α-Fe_2O_3 on the ketonic fraction is not significant, as shown in **Figure 10**. More specifically, all applied catalysts were found to promote the formation of 2-hydroxy-2-cyclopenten-1-one at the expense of 1,2-cyclopentanedione, possibly through a hydrogenation route. The hydrogen supplied to this reaction originates from the original biomass decomposition reactions and further enhanced through subsequent water-gas shift reactions over the iron oxide catalysts. In addition, the formation of 1-hydroxy-2-propanone, which is associated with the decomposition of the cellulosic fraction of biomass, is partially suppressed by the mono- and dual-sized nanoparticle-containing catalysts. In contrast, the mono-sized micro-particles do not display any noticeable effect.

Impact on the Distribution of Acidic Compounds

The distribution of acidic compounds resulting from the application of various catalyst particle sizes and mixtures is shown in **Figure 11**. In general terms, the application of the iron oxide catalysts does not significantly affect the total relative peak area of the acidic groups. However, it has a noticeable effect on the relative distribution of the light (aliphatic acids with $C \leq 4$) and heavy (aliphatic and cyclic acids with $C > 4$) acids. It can be generally observed that the application of the α-Fe_2O_3 catalysts results in the decrease of the heavy fraction of the acidic compound. This is significantly more intense for the monosized FS054, and FSm002 catalysts, whilst all FS221 containing catalysts display a relatively moderate behavior with only a minor decrease on the relative peak area of the heavy acids. However, no definite conclusion can be drawn since the error in the reproducibility experiments for the FS221 catalyst on the light acids is relatively large.

Generally, it can be considered that particle size does not significantly affect the distribution of light and heavy acidic compounds in the CFP of pinewood. Although the monosized catalysts, FS054, FS221, and FSm002 have significantly different specific surface areas and pore sizes (**Table 1**), there is no evidence to support the hypothesis that those parameters would have any major effect. The conversion of acids is probably primarily dependent on particle shape, considering the moderate effects of the dual-sized catalyst mixtures on the final distribution and their lower capacity to increase the light acid fraction. In addition, competing reactions on the more defective and anisotropically shaped spherical catalyst mixtures might further inhibit the conversion of long-chain aliphatic acids.

CONCLUSION

Mono- and dual-sized α-Fe_2O_3 catalysts were prepared and tested as potential catalysts in pinewood biomass's thermochemical processing (fast pyrolysis). With the increase in the particle size from 54 nm to 2 μm the specific surface area of powders decreases about eight times. The ratio of mesoporosity to microporosity changes with the size variation. All catalysts contain carbon at the surface, and the highest amount was revealed for FS054 catalyst. The maximum oxygen and iron surface concentration were revealed for FS054-FS221 and FS221-FSm002 catalyst respectively. It was shown that different catalyst sizes and catalyst mixtures have a noticeable effect on the resulting product distribution. It was observed that the application of α-Fe_2O_3 had a potent effect on reducing the phenolic fraction, possibly through the radical formation favoring charring and coking reactions. However, it was demonstrated that the catalyst particle size or mixture showed a specific preference for different phenolic compounds. All applied catalysts displayed a high selectivity towards the formation of acetaldehyde through the levoglucosan decomposition pathway. However, the dual-sized catalyst FS054-FS221 showed a diverse effect by eliminating acetaldehyde due to the effective anisotropic catalyst particle mixture or a catalytic transfer hydrogenation reaction targeting the terminal carbonyl of the molecule. The high CO_2 release observed in this case further supported the decarbonylation with subsequent water-gas shift reaction over the Fe_2O_3 hypothesis. All applied catalysts showed an insignificant effect on the ketonic fraction distribution. The most notable reaction was the promotion of the formation of 2-hydroxy-2-cyclopenten-1-one at the expense of 1,2-cyclopentanedione, possibly through a hydrogenation route. Finally, it was observed that all applied catalysts had a noticeable effect on the reduction of the heavy acids ($C > 4$) in the final acidic product distribution. However, there was no substantial evidence that catalyst particle sizes and their associated microstructural parameters, such as pore size and surface area, play any significant role in the heavy and light acid distribution. FS054 and FSm002 catalysts showed good chemical and phase stability. FS054-FS221 catalyst demonstrates very promising catalytic behavior for incorporation into industrial-scale thermochemical processing, but the oxidation activity of the Fe^{3+}/Fe^{2+} pair must be improved to avoid the polymorph transformation and reach its phase stability.

DATA AVAILABILITY STATEMENT

The raw data supporting the conclusion of this article will be made available by the authors, without undue reservation.

AUTHOR CONTRIBUTIONS

Investigation, AB; supervision, KP and EK; writing—original draft, AB, KP and EK.

ACKNOWLEDGMENTS

The authors gratefully acknowledge Mr. Lan Jian Zhuge for XPS measurements and Dr. Zhu Xing (Testing and Analysis Center, Soochow University, China) for TEM images and for financial support the SIP JinjiLake Double-Hundred Talents Program (01414892X/2012-00460) and Research Development Funds (RDF-13-02-14, RDF-13-03-06) at Xi'an Jiaotong-Liverpool University.

REFERENCES

Alayont, Ş., Kayan, D. B., Durak, H., Alayont, E. K., and Genel, S. (2022). The Role of Acidic, Alkaline and Hydrothermal Pretreatment on Pyrolysis of Wild Mustard (Sinapis Arvensis) on the Properties of Bio-Oil and Bio-Char. *Bioresour. Techn. Rep.* 17, 100980. doi:10.1016/j.biteb.2022.100980

Asmadi, M., Kawamoto, H., and Saka, S. (2011). Thermal Reactivities of Catechols/pyrogallols and Cresols/xylenols as Lignin Pyrolysis Intermediates. *J. Anal. Appl. Pyrolysis* 92, 76–87. doi:10.1016/j.jaap.2011.04.012

Aysu, T., and Durak, H. (2015). Catalytic Pyrolysis of Liquorice (Glycyrrhiza Glabra L.) in a Fixed-Bed Reactor: Effects of Pyrolysis Parameters on Product Yields and Character. *J. Anal. Appl. Pyrolysis* 111, 156–172. doi:10.1016/j.jaap.2014.11.017

Baimoldina, A., Papadikis, K., and Konysheva, E. Yu. (2019). Diverse Impact of α-Fe_2O_3 with Nano/micro-Sized Shapes on the Catalytic Fast Pyrolysis of Pinewood: Py-GC/MS Study. *J. Anal. Appl. Pyrolysis* 139, 145–155. doi:10.1016/j.jaap.2019.01.019

Barrett, E. P., Joyner, L. G., and Halenda, P. P. (1951). The Determination of Pore Volume and Area Distributions in Porous Substances. I. Computations from Nitrogen Isotherms. *J. Am. Chem. Soc.* 73, 373–380. doi:10.1021/ja01145a126

Bridgwater, A. V. (2012). Review of Fast Pyrolysis of Biomass and Product Upgrading. *Biomass Bioenergy* 38, 68–94. doi:10.1016/j.biombioe.2011.01.048

Demirbas, A. (2000). Mechanisms of Liquefaction and Pyrolysis Reactions of Biomass. *Energ. Convers. Manage.* 41, 633–646. doi:10.1016/S0196-8904(99)00130-2

Dubinin, M. M. (1966). *Chemistry and Physics of Carbon*. Editor P. L. Walker (New York: Marcel Dekker), 2, 51–120.

Fouad, D. E., Zhang, C., Mekuria, T. D., Bi, C., Zaidi, A. A., and Shah, A. H. (2019). Effects of Sono-Assisted Modified Precipitation on the Crystallinity, Size, Morphology, and Catalytic Applications of Hematite (α-Fe_2O_3) Nanoparticles: A Comparative Study. *Ultrason. Sonochem.* 59, 104713. doi:10.1016/j.ultsonch.2019.104713

Grosvenor, A. P., Kobe, B. A., Biesinger, M. C., and McIntyre, N. S. (2004). Investigation of Multiplet Splitting of Fe 2p XPS Spectra and Bonding in Iron Compounds. *Surf. Interf. Anal.* 36, 1564–1574. doi:10.1002/sia.1984

Gupta, J., Papadikis, K., Kozhevnikov, I. V., and Konysheva, E. Yu. (2017). Exploring the Potential of Red Mud and Beechwood Co-processing for the Upgrading of Fast Pyrolysis Vapours. *J. Anal. Appl. Pyrolysis* 128, 35–43. doi:10.1016/j.jaap.2017.11.002

Heinrich, V. E., and Cox, P. A. (1994). *The Surface Science of Metal Oxides*. Cambridge: Cambridge University Press, 227.

Horvath, G., and Kawazoe, K. (1983). Method for the Calculation of Effective Pore Size Distribution in Molecular Sieve Carbon. *J. Chem. Eng. Jpn.* 16, 470–475. doi:10.1252/jcej.16.470

Hu, X., and Gholizadeh, M. (2019). Biomass Pyrolysis: A Review of the Process Development and Challenges from Initial Researches up to the Commercialisation Stage. *J. Energ. Chem.* 39, 109–143. doi:10.1016/j.jechem.2019.01.024

Isahak, W. N. R. W., Hisham, M. W. M., Yarmo, M. A., and Yun Hin, T.-y. (2012). A Review on Bio-Oil Production from Biomass by Using Pyrolysis Method. *Renew. Sustain. Energ. Rev.* 16, 5910–5923. doi:10.1016/j.rser.2012.05.039

Jia, Z., Liu, J., Wang, Q., Li, S., Qi, Q., and Zhu, R. (2015). Synthesis of 3D Hierarchical Porous Iron Oxides for Adsorption of Congo Red from Dye Wastewater. *J. Alloys Compd.* 622, 587–595. doi:10.1016/j.jallcom.2014.10.125

Kastner, J. R., Hilten, R., Weber, J., McFarlane, A. R., Hargreaves, J. S. J., and Batra, V. S. (2015). Continuous Catalytic Upgrading of Fast Pyrolysis Oil Using Iron Oxides in Red Mud. *RSC Adv.* 5 (37), 29375–29385. doi:10.1039/c5ra01548k

Kawamoto, H. (2017). Lignin Pyrolysis Reactions. *J. Wood Sci.* 63, 117–132. doi:10.1007/s10086-016-1606-z

Li, P., Shi, X., Wang, X., Song, J., Fang, S., Bai, J., et al. (2021). Bio-oil from Biomass Fast Pyrolysis: Yields, Related Properties and Energy Consumption Analysis of the Pyrolysis System. *J. Clean. Prod.* 328, 129613. doi:10.1016/j.jclepro.2021.129613

Liang, X., Wang, L., Wen, T., Liu, H., Zhang, J., Liu, Z., et al. (2022). Mesoporous Poorly Crystalline α-Fe_2O_3 with Abundant Oxygen Vacancies and Acid Sites for Ozone Decomposition. *Sci. Total Environ.* 804 (12), 150161. doi:10.1016/j.scitotenv.2021.150161

Lim, X., Sanna, A., and Andrésen, J. M. (2014). Influence of Red Mud Impregnation on the Pyrolysis of Oil palm Biomass-EFB. *Fuel* 119, 259–265. doi:10.1016/j.fuel.2013.11.057

Liu, C., Wang, H., Karim, A. M., Sun, J., and Wang, Y. (2014). Catalytic Fast Pyrolysis of Lignocellulosic Biomass. *Chem. Soc. Rev.* 43 (22), 7594–7623. doi:10.1039/c3cs60414d

Lu, Q., Zhang, Z.-F., Dong, C.-Q., and Zhu, X.-F. (2010). Catalytic Upgrading of Biomass Fast Pyrolysis Vapors with Nano Metal Oxides: An Analytical Py-GC/MS Study. *Energies* 3 (11), 1805–1820. doi:10.3390/en3111805

Lynd, L. R., Cushman, J. H., Nichols, R. J., and Wyman, C. E. (1991). Fuel Ethanol from Cellulosic Biomass. *Science* 251, 1318–1323. doi:10.1126/science.251.4999.1318

Mabate, T. P., Meijboom, R., and Bingwa, N. (2022). The Inorganic Perovskite-Catalyzed Transfer Hydrogenation of Cinnamaldehyde Using Glycerol as a Hydrogen Donor. *Catalysts* 12, 241. doi:10.3390/catal12020241

Machado, A. d. S., Mexias, A. S., Vilela, A. C. F., and Osorio, E. (2013). Study of Coal, Char and Coke Fines Structures and Their Proportions in the Off-Gas Blast Furnace Samples by X-ray Diffraction. *Fuel* 114, 224–228. doi:10.1016/j.fuel.2012.07.064

Machala, L., Tuček, J., and Zbořil, R. (2011). Polymorphous Transformations of Nanometric Iron(III) Oxide: A Review. *Chem. Mater.* 23 (14), 3255–3272. doi:10.1021/cm200397g

Mendes, F. L., Ximenes, V. L., de Almeida, M. B. B., Azevedo, D. A., Tessarolo, N. S., and de Rezende Pinho, A. (2016). Catalytic Pyrolysis of Sugarcane Bagasse and Pinewood in a Pilot Scale Unit. *J. Anal. Appl. Pyrolysis* 122, 395–404. doi:10.1016/j.jaap.2016.08.001

Meng, F., Li, J., Cushing, S. K., Bright, J., Zhi, M., Rowley, J. D., et al. (2013). Photocatalytic Water Oxidation by Hematite/reduced Graphene Oxide Composites. *ACS Catal.* 3, 746–751. doi:10.1021/cs300740e

Papadikis, K., Gu, S., and Bridgwater, A. V. (2009). CFD Modelling of the Fast Pyrolysis of Biomass in Fluidised Bed Reactors: Modelling the Impact of Biomass Shrinkage. *Chem. Eng. J.* 149 (1–3), 417–427. doi:10.1016/j.cej.2009.01.036

Rufus, A., Sreeju, N., and Philip, D. (2019). Size Tunable Biosynthesis and Luminescence Quenching of Nanostructured Hematite (α-Fe_2O_3) for Catalytic Degradation of Organic Pollutants. *J. Phys. Chem. Sol.* 124, 221–234. doi:10.1016/j.jpcs.2018.09.026

Schwertmann, U., and Cornell, R. M. (2000). *Iron Oxides in the Laboratory: Preparation and Characterisation*. 2nd ed. Weinheim: Wiley VCH, 188.

Song, Q., Zhao, H., Ma, Q., Yang, L., Ma, L., Wu, Y., et al. (2022). Catalytic Upgrading of Coal Volatiles with Fe_2O_3 and Hematite by TG-FTIR and Py-GC/MS. *Fuel* 313, 122667. doi:10.1016/j.fuel.2021.122667

Torri, C., Reinikainen, M., Lindfors, C., Fabbri, D., Oasmaa, A., and Kuoppala, E. (2010). Investigation on Catalytic Pyrolysis of pine Sawdust: Catalyst Screening by Py-GC-MIP-AED. *J. Anal. Appl. Pyrolysis* 88 (1), 7–13. doi:10.1016/j.jaap.2010.02.005

Tuček, J., Machala, L., Ono, S., Namai, A., Yoshikiyo, M., Imoto, K., et al. (2015). Zeta-Fe_2O_3 - A New Stable Polymorph in Iron(III) Oxide Family. *Sci. Rep.* 5, 15091. doi:10.1038/srep15091

Velden, M. V. D., Baeyens, J., Brems, A., Janssens, B., and Dewil, R. (2010). Fundamentals, Kinetics and Endothermicity of the Biomass Pyrolysis Reaction. *Renew. Energ.* 35 (1), 232–242. doi:10.1016/j.renene.2009.04.019

Walker, J., Stragauzzi, G. I., Manogue, W. H., and Schuit, G. C. A. (1988). Carbon Monoxide and Propene Oxidation by Iron Oxides for Auto-Emission Control. *J. Catal.* 110, 298–309. doi:10.1016/0021-9517(88)90321-1

Weber, J., Thompson, A., Wilmoth, J., Batra, V. S., Janulaitis, N., and Kastner, J. R. (2019). Effect of Metal Oxide Redox State in Red Mud Catalysts on Ketonization of Fast Pyrolysis Oil Derived Oxygenates. *Appl. Catal. B: Environ.* 241, 430–441. doi:10.1016/j.apcatb.2018.08.061

Xu, Q., Liu, Z., Jiang, H., Zhang, Q., Zan, C., Ma, D., et al. (2017). Chemical-structural Properties of the Coke Produced by Low Temperature Oxidation Reactions during Crude Oil *In-Situ* Combustion. *Fuel* 207, 179–188. doi:10.1016/j.fuel.2017.06.026

Yamamoto, S., Kendelewicz, T., Newberg, J. T., Ketteler, G., Starr, D. E., Mysak, E. R., et al. (2010). Water Adsorption on α-Fe_2O_3(0001) at Near Ambient Conditions. *J. Phys. Chem. C* 114, 2256–2266. doi:10.1021/jp909876t

Yücedağ, E., and Durak, H. (2019). Bio-oil and Bio-Char from Lactuca Scariola: Significance of Catalyst and Temperature for Assessing Yield and Quality of Pyrolysis. *Energy Sourc. A Recovery Util. Environ. Effects*, 1–14. doi:10.1080/15567036.2019.1645765

Zhang, Q., Chang, J., Wang, T., and Xu, Y. (2007). Review of Biomass Pyrolysis Oil Properties and Upgrading Research. *Energ. Convers. Manage.* 48, 87–92. doi:10.1016/j.enconman.2006.05.010

Zhang, X., Yang, W., and Blasiak, W. (2012). Thermal Decomposition Mechanism of Levoglucosan during Cellulose Pyrolysis. *J. Anal. Appl. Pyrolysis* 96, 110–119. doi:10.1016/j.jaap.2012.03.012

Zhang, X., Sun, L., Chen, L., Xie, X., Zhao, B., Si, H., et al. (2014). Comparison of Catalytic Upgrading of Biomass Fast Pyrolysis Vapors over CaO and Fe(III)/CaO Catalysts. *J. Anal. Appl. Pyrolysis* 108, 35–40. doi:10.1016/j.jaap.2014.05.020

Zheng, Y., Cheng, Y., Wang, Y., Bao, F., Zhou, L., Wei, X., et al. (2006). Quasicubic α-Fe_2O_3 Nanoparticles with Excellent Catalytic Performance. *J. Phys. Chem. B* 110, 3093–3097. doi:10.1021/jp056617q

Conflict of Interest: The authors declare that the research was conducted in the absence of any commercial or financial relationships that could be construed as a potential conflict of interest.

Publisher's Note: All claims expressed in this article are solely those of the authors and do not necessarily represent those of their affiliated organizations, or those of the publisher, the editors and the reviewers. Any product that may be evaluated in this article, or claim that may be made by its manufacturer, is not guaranteed or endorsed by the publisher.